AD-A173 492 A BARELY IMPLICIT CORRECTION FOR FLUX-CORRECTED TRANSPORT(U) NAVAL RESEARCH LAB WASHINGTON DC G PATNAIK ET AL 30 SEP 86 NRL-MR-5855 1/1

UNCLASSIFIED F/G 20/4 NL

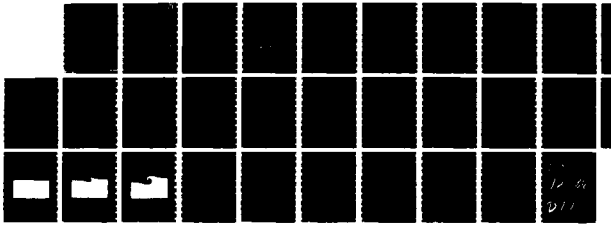

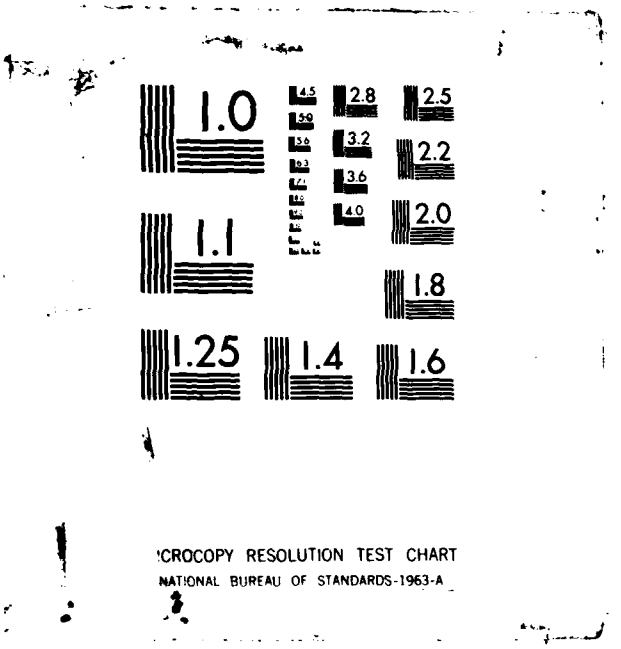
1.0
1.1
1.25
1.4
1.6
1.8
2.0
2.2
2.5
2.8
3.2
3.6
4.0
4.5
5.0
5.6
6.3
ICROCOPY RESOLUTION TEST CHART
NATIONAL BUREAU OF STANDARDS-1963-A

Naval Research Laboratory

Washington, DC 20375-5000 NRL Memorandum Report 5855 September 30, 1986

A Barely Implicit Correction for Flux-Corrected Transport

G. PATNAIK,* R. H. GUIRGUIS,* J. P. BORIS,
AND E. S. ORAN

Laboratory for Computational Physics

**Berkeley Research Associates*
Springfield, VA 22150

Approved for public release; distribution unlimited.

SECURITY CLASSIFICATION OF THIS PAGE

ADA173492

REPORT DOCUMENTATION PAGE

1a. REPORT SECURITY CLASSIFICATION UNCLASSIFIED	1b. RESTRICTIVE MARKINGS
2a. SECURITY CLASSIFICATION AUTHORITY	3. DISTRIBUTION/AVAILABILITY OF REPORT Approved for public release; distribution unlimited.
2b. DECLASSIFICATION/DOWNGRADING SCHEDULE	
4. PERFORMING ORGANIZATION REPORT NUMBER(S) NRL Memorandum Report 5855	5. MONITORING ORGANIZATION REPORT NUMBER(S)
6a. NAME OF PERFORMING ORGANIZATION Naval Research Laboratory 6b. OFFICE SYMBOL (If applicable)	7a. NAME OF MONITORING ORGANIZATION
6c. ADDRESS (City, State, and ZIP Code) Washington, DC 20375-5000	7b. ADDRESS (City, State, and ZIP Code)
8a. NAME OF FUNDING/SPONSORING ORGANIZATION Office of Naval Research 8b. OFFICE SYMBOL (If applicable)	9. PROCUREMENT INSTRUMENT IDENTIFICATION NUMBER
8c. ADDRESS (City, State, and ZIP Code) Arlington, VA 22203	10. SOURCE OF FUNDING NUMBERS PROGRAM ELEMENT NO. 61153N; PROJECT NO. 44-1530-06; TASK NO. RR011-09-43; WORK UNIT ACCESSION NO. DN280-071

11. TITLE (Include Security Classification)
A Barely Implicit Correction for Flux-Corrected Transport

12. PERSONAL AUTHOR(S)
Patnaik,* G., Guirguis,* R.H., Boris, J.P., and Oran, E.S.

13a. TYPE OF REPORT	13b. TIME COVERED FROM ____ TO ____	14. DATE OF REPORT (Year, Month, Day)	15. PAGE COUNT
		1986 September 30	36

16. SUPPLEMENTARY NOTATION
*Berkeley Research Associates
Springfield, VA 22150

17. COSATI CODES			18. SUBJECT TERMS (Continue on reverse if necessary and identify by block number)
FIELD	GROUP	SUB-GROUP	Flux-corrected transport; Low speed flow; Barely implicit correction

19. ABSTRACT (Continue on reverse if necessary and identify by block number)

(FCT)

The Barely Implicit Correction, or BIC, is a technique to remove the stringent limit on the timestep imposed by the sound speed in explicit methods. This is done by adding one elliptic equation which has to be solved implicitly. BIC is combined with the Flux-Corrected Transport algorithm in order to represent sharp gradients in subsonic flows accurately. The resultant algorithm costs about the same per timestep as a single explicit timestep calculated using an optimized FCT module. Several examples show the technique's ability to solve nearly incompressible flows very economically. — to p. 1.

20. DISTRIBUTION/AVAILABILITY OF ABSTRACT	21. ABSTRACT SECURITY CLASSIFICATION
☒ UNCLASSIFIED/UNLIMITED ☐ SAME AS RPT. ☐ DTIC USERS	UNCLASSIFIED

22a. NAME OF RESPONSIBLE INDIVIDUAL	22b. TELEPHONE (Include Area Code)	22c. OFFICE SYMBOL
Elaine S. Oran	(202) 767-2960	Code 4040

DD FORM 1473, 84 MAR 83 APR edition may be used until exhausted. All other editions are obsolete

SECURITY CLASSIFICATION OF THIS PAGE

CONTENTS

A BARELY IMPLICIT CORRECTION FOR FLUX-CORRECTED TRANSPORT

I. INTRODUCTION

The solution of time dependent compressible flow problems is complicated by conflicting requirements of mathematical accuracy, nonlinearity, physical conservation and positivity. This is especially true near discontinuities where "accurate" high order algorithms produce ripples while linear monotonic (i.e. positivity preserving) schemes are highly diffusive. After Godunov [1] showed that a linear algorithm ensures positivity only if it is first order, the next logical step was to look at nonlinear methods to develop effectively higher order, more accurate monotonic schemes. The first high-order monotone algorithm (Boris [2]) was designed to maintain local positivity near steep gradients while keeping a high order of accuracy elsewhere. The major principles of the monotone high order algorithms are that they maintain positivity through a procedure that uses a nonlinear combination of diffusive and antidiffusive fluxes. The Flux-Corrected Transport (FCT) algorithm that we use in this paper [3, 4] is made fourth order by the appropriate subtraction of corrected fluxes. Other monotone methods have been reviewed by Woodward and Collela [5] and Baer [6]. In this paper we confine our discussions to a Barely Implicit Correction (BIC) to FCT. BIC is also extendable to other monotone methods.

Positivity-preserving monotone FCT methods were developed to calculate shocks accurately. Even for subsonic flows with discontinuities, their high accuracy produced much better solutions than standard finite difference techniques. The early FCT methods were explicit. No serious limitation arose from the explicitness in supersonic flows because the major features of interest in the flow move at about the sound speed. Using these methods for subsonic flows, however, is economical only if the characteristic velocities in the flow field are a reasonable fraction of the speed of sound [7, 8] or if the fast sound waves are mathematically removed from the system of equations.

Manuscript approved June 26, 1986.

The Barely Implicit Correction described in this paper was motivated by the need to calculate subsonic flows accurately in which the velocities of the important flow structures are much lower than the speed of sound. In typical cases, we are interested in flow velocities from centimeters to tens of meters per second. These flow velocities are encountered, for example, in laminar flames and low-speed fuel injection in engines. Our objectives are to remove the timestep limit imposed by the speed of sound, retain the accuracy required to resolve the detailed features of the flow, and reduce the computational costs.

The obvious way to beat the sound-speed limit on the timestep is to make the calculation implicit. This has been done successfully for many linear methods, such as the MacCormack method [9], the Beam and Warming method [10], and the ICE and RICE methods of Hirt and Cook [11]. In addition, recent developments have been reported for implicit, nonlinear PPM [12] and TVD [13] methods. A major problem with all of these methods is that they are relatively expensive, even though they can be made relatively accurate.

Another approach is the asymptotic methods. Examples of these are the methods developed by Jones and Boris [14], Rehm and Baum [15] and Paolucci [16]. In these methods, the only effects of compression that are allowed are the changes in density due to heating or cooling. Pressure fluctuations are filtered out, thus removing the timestep limit imposed by the sound speed. However, other effects from sound waves are removed in this process.

A a useful approach was given by Casulli and Greenspan [17]. Their analysis indicated that it is not necessary to treat all of the terms in the gas dynamic equations implicitly to be able to use longer timesteps than those dictated by explicit stability limits. Only those explicit terms which force this limit need to be treated implicitly.

The algorithm presented in this paper has two steps. The first step is explicit. It is performed at a large timestep governed by a CFL condition on the fluid velocity. This step should be done with an accurate nonlinear monotone method, and we have used FCT in the examples given. The second step is an implicit correction step requiring the solution of one elliptic equation for the pressure correction. The term "Barely Implicit Correction" emphasizes our use

of the idea of Casulli and Greenspan, that only certain terms must be treated implicitly.

The total cost per timestep of BIC-FCT is about the same as for a full explicit FCT step. Thus the cost of a complete calculation is one or two orders of magnitude below that required if a very slow flow were treated explicitly. Since only one elliptic equation is solved, the method is considerably faster than many implicit methods commonly used. In addition, using a nonlinear monotone method for the explicit step ensures high accuracy.

II. METHOD OF SOLUTION

Derivation of the Barely Implicit Correction

We are solving the compressible gas dynamics conservation equations for density ρ, momentum density $\rho\mathbf{v}$, and total internal energy, E,

$$\frac{\partial \rho}{\partial t} = -\nabla \cdot \rho\mathbf{v} , \tag{1}$$

$$\frac{\partial \rho\mathbf{v}}{\partial t} = -\nabla \cdot \rho\mathbf{v}\mathbf{v} - \nabla P , \tag{2}$$

$$\frac{\partial E}{\partial t} = -\nabla \cdot (E + P)\mathbf{v} , \tag{3}$$

where the total energy density E is

$$E = \epsilon + \frac{1}{2}\rho\mathbf{v}^2. \tag{4}$$

The equation of state relating pressure and internal energy is

$$P = (\gamma - 1)\epsilon . \tag{5}$$

In a recent paper, Casulli and Greenspan [17] showed that it is not necessary to treat every term in a finite-difference algorithm implicitly to avoid the timestep constraint imposed by the Courant condition. Further, they showed that only those terms containing the pressure in Eq. (2) and the velocity in Eq. (3) must be treated implicitly. Their paper provides the starting concepts for the work we present. In addition, we have extended their analysis to include an implic-

itness parameter, ω, that can be used to vary the degree of implicitness of the algorithm. In general, we can have $0.5 \leq \omega \leq 1$, where the implicit terms are centered in time for $\omega = 0.5$. For $\omega < 0.5$, the method is found to be unstable for sufficiently large timesteps.

There are two stages to the algorithm. One stage is an explicit predictor that determines the provisional values $\tilde{\rho}$ and $\tilde{\mathbf{v}}$,

$$\frac{\tilde{\rho} - \rho^o}{\Delta t} = -\nabla \cdot \rho^o \mathbf{v}^o , \tag{6}$$

$$\frac{\tilde{\rho}\tilde{\mathbf{v}} - \rho^o \mathbf{v}^o}{\Delta t} = -\nabla \cdot \rho^o \mathbf{v}^o \mathbf{v}^o - \nabla P^o , \tag{7}$$

The tilde denotes predictor values at the new time, and the superscripts o and n are used to denote the old time and new time, respectively. So far only time has been differenced, not space. The implicit forms of Eqs. (2) and (3) are

$$\frac{\rho^n \mathbf{v}^n - \rho^o \mathbf{v}^o}{\Delta t} = -\nabla \cdot \rho^o \mathbf{v}^o \mathbf{v}^o - \nabla[\omega P^n + (1-\omega) P^o] , \tag{8}$$

$$\frac{E^n - E^o}{\Delta t} = -\nabla \cdot (E^o + P^o)[\omega \mathbf{v}^n + (1-\omega)\mathbf{v}^o] , \tag{9}$$

where ω is the implicitness parameter discussed above. When $\omega = 1$, the algorithm is completely implicit and reverts to the original equations analyzed by Casulli and Greenspan.

We can reduce this implicit system to only one equation by eliminating $\mathbf{v}^n$ between Eq. (8) and (9). To do this, we first define the change in pressure, δP, as

$$\delta P \equiv \omega(P^n - P^o) . \tag{10}$$

Then the correction equation for momentum can be obtained in terms of δP by subtracting Eq. (7) from Eq. (8),

$$\frac{\rho^n \mathbf{v}^n - \tilde{\rho}\tilde{\mathbf{v}}}{\Delta t} = -\nabla \omega (P^n - P^o) = -\nabla \delta P . \tag{11}$$

We obtain the new velocity by rearranging Eq. (11) and letting $\rho^n = \tilde{\rho}$, so that

$$\mathbf{v}^n = -\frac{\Delta t}{\tilde{\rho}} \nabla \delta P + \tilde{\mathbf{v}} . \tag{12}$$

We obtain a correction equation for energy using the equation of state with γ constant, Eq. (4),

$$\epsilon^n = \frac{\delta P}{(\gamma-1)\omega} + \epsilon^o \,, \tag{13}$$

where the ω factor appears from the definition of δP. We find δP by substituting Eqs. (12) and (13) into Eq. (9),

$$\begin{aligned} \frac{\tilde{\rho}\tilde{\mathbf{v}}^2 - \rho^o \mathbf{v}^{o2}}{2\Delta t} + \frac{\delta P}{(\gamma-1)\omega\Delta t} &= \omega\Delta t\, \nabla\cdot\left(\frac{E^o+P^o}{\tilde{\rho}}\right)\nabla\delta P \\ &\quad - \omega\nabla\cdot(E^o+P^o)\tilde{\mathbf{v}} \\ &\quad - (1-\omega)\nabla\cdot(E^o+P^o)\mathbf{v}^o \,. \end{aligned} \tag{14}$$

Note that the kinetic energy change is included explicitly. For convenience, we define the quantity $\overline{E}$,

$$\frac{\overline{E}-E^o}{\Delta t} \equiv -\nabla\cdot(E^o+P^o)\left[\omega\tilde{\mathbf{v}} + (1-\omega)\mathbf{v}^o\right] \,. \tag{15}$$

This allows us to rewrite Eq. (14),

$$\frac{\delta P}{(\gamma-1)\omega\Delta t} - \omega\Delta t\,\nabla\cdot\left(\frac{E^o+P^o}{\tilde{\rho}}\right)\nabla\delta P = \frac{\overline{E}-E^o}{\Delta t} - \frac{\tilde{\rho}\tilde{\mathbf{v}}^2 - \rho^o\mathbf{v}^{o2}}{2\Delta t} \tag{16}$$

which provides us with an elliptic equation for δP. The right hand side of Eq. (16) is evaluated explicitly using Eq. (15). After the elliptic equation is solved for δP, momentum and energy are corrected by Eqs. (11) and (13). Note that we started with two equations with implicit terms, and now we have reduced it to one equation, Eq. (16).

The Barely Implicit Correction is carried out in three stages. In the first, Eqs. (6), (7), and (15) are integrated with any one-step explicit method. The pressure correction equation, Eq. (16) is solved by an elliptic solver in the second stage. The last stage requires the use of Eqs. (11) and (13) to obtain the final values of momentum and energy at the new timestep.

Solution Procedure

The derivation given above does not involve any specific choice of method for differencing the spatial derivatives. The only restriction so far is that the spatial derivatives must be evaluated at the appropriate time levels indicated

by the superscripts. This allows great flexibility in the choice of the differencing scheme for these terms. Thus we can integrate the explicit predictor equations, Eqs. (6), (7), and (15) with FCT. This gives us the benefits of using a high-order monotone method. We have given the name BIC-FCT to this particular combination of BIC and FCT. Tests, such as those presented below, indicate that it has the same accuracy and flexibility as FCT.

At each timestep, the solution procedure we have implemented is divided into the three stages:

1. Explicit predictor stage

The density and momentum are advanced explicitly as specified by Eqs. (6) and (7) using FCT. This produces the intermediate quantities, $\tilde{\rho}$ and $\tilde{\rho}\tilde{\mathbf{v}}$. The $\tilde{\mathbf{v}}$ is found from $\tilde{\rho}\tilde{\mathbf{v}}/\tilde{\rho}$. Then $\tilde{\mathbf{v}}$ is used to obtain $\overline{E}$ given by Eq. (15). FCT is also used to obtain $\overline{E}$.

2. Solution of Eq. (16) for δP

In one dimension, the solution to the difference form of Eq. (16) requires the solution of a system of linear equations by a tridiagonal matrix solver. In two dimensions, the solution requires an elliptic solver. For the two-dimensional calculations shown below, we used a multigrid method [18]. A substantial part of the computer time required in this stage is in setting up the coefficients for an elliptic equation solver.

3. Momentum and energy corrections

These corrections are obtained from the pressure change δP using Eqs. (11) and (13), respectively. These corrected values and the density obtained explicitly in the first stage are the starting conditions at the new timestep.

These three stages are carried out at every timestep. The derivatives in the pressure difference equation, Eq. (16), are approximated by central differences. All physical quantities are calculated at cell centers, and those values needed at cell interfaces are obtained by averaging.

This technique can be implemented in one, two, or three dimensions. In one and two dimensions, several different geometries are possible. For example, we have implemented two-dimensional planar and axisymmetric geometries, and one-dimensional Cartesian, cylindrical, and spherical. Any boundary conditions

that are commonly used with the standard FCT modules can be used with this algorithm [7].

III. TESTS OF THE METHOD

Advection of a One-Dimensional Contact Discontinuity

The problem we consider first is the flow of air through a duct in one dimension. The duct is initially filled with air at standard temperature and pressure. Then cold air with twice the density flows into the duct. There is a contact discontinuity at the location where the cold, dense air and normal air meet. In the absence of diffusive processes, the contact discontinuity should move at the velocity of the incoming air. This numerical test shows the ability of BIC-FCT to propagate a contact discontinuity with the same accuracy as FCT.

The computational domain was divided into 200 evenly spaced cells of 1 cm. Initially, the discontinuity was 0.1 m from the inlet. The flow velocity of air in the duct was 10 m/s. The inlet conditions corresponding to the cold air are held fixed throughout the calculation.

The timestep used in this calculation is 0.5 ms, which is the time required for the fluid to cross half a cell. This should be compared to the Courant limit of 24 μs. Typical explicit methods are forced to employ a timestep of less than half of the Courant limit to control the growth of of perturbations in pressure and velocity. In this example, a factor of forty to fifty is gained over the explicit timestep.

Figure 1 shows the density profiles at intervals of fifty steps. The discontinuity, initially across one cell, spreads to three or four cells as it moves across the system. Most important, however, is that the discontinuity spreads no further throughout the course of the solution and there are no ripples in the solutions. Both of these features are in the underlying explicit FCT algorithm. The results presented in the figure were obtained with $\omega = 1$. The influence of sound waves in this problem are negligible, so that any stable value of ω gives the same result.

Sound Wave Damping

In most finite-difference methods, high-frequency sound waves are attenuated. Implicit methods, however, tend to damp all frequencies, with the lower frequencies damped least. The problem we now present tests the sound-wave damping in BIC-FCT.

We consider a closed, one-dimensional pipe 1 m long in which the fluid velocity was initialized with a sinusoidal variation. The maximum amplitude of the variation was 1 m/s at the center of the pipe. Effectively, the initial conditions correspond to a sound wave in the pipe with a wavelength of 2 m.

Each curve in Fig. 2 shows the fluid velocity at the center of the pipe as a function of the number of cycles for a different value of ω. The damping is greatest when $\omega = 1$, which is when the method is completely implicit. The damping decreases as ω is reduced, and it becomes negligble when $\omega = 0.5$. Any further reduction in ω leads to instability of the numerical method. We conclude that the amount of damping is a strong function of implicitness parameter. The results shown in Fig. 2 were for a sound wave with a cell size of 2.5 cm using a timestep of 0.1 msec.

The dispersion relation, obtained directly from the calculations, is shown in Fig. 3a for $CFL = 0.5$. The CFL number is defined as

$$CFL = \frac{\text{sound speed} \times \text{time step}}{\text{cell size}}.$$

These calculations were made by varying the timestep as well as the number of cells in the 1 m pipe. The product of the wave number, k, and the cell size Δx is inversely related to the accuracy of representation of the wave. The number of cells per wavelength is given by

$$N = \frac{2\pi}{k\Delta x}.$$

On the vertical axis, we show ω_d and ω_t, the observed and theoretical frequencies of the wave. A totally dispersion free algorithm, in which $\omega_d = \omega_t$, would yield the 45 degree line shown. Curves for different values of the implicitness

parameter are presented. For comparison purposes, the results for the explicit, predictor-corrector JPBFCT method [4] are included. JPBFCT requires two applications of the FCT algorithm at each timestep. This two-step process makes JPBFCT second order in time.

Figure 3b indicates the change in amplitude of the wave in one period. The amplification is always less than unity, indicating that the wave is damped. If the amplification were greater than unity, the calculation would be unstable. As expected, damping increases when the method is more implicit. Poorly resolved wavelengths are damped, even by the fully explicit method. It should be noted that BIC-FCT with $\omega = 0.55$ performs nearly as well as the explicit JBPFCT. Values of ω nearer 0.5 brings results of the two methods even closer.

Figures 4a, 4b and 5a, 5b give the dispersion relation and damping for $CFL = 2$ and $CFL = 10$ respectively. Representation of the sound wave deteriorates more rapidly as resolution is lost for these CFLs. Curves for $CFL = 10$ are shorter than those for lower CFL because the timestep becomes too large to resolve the oscillatory nature of the wave.

This example points out the need for caution when attempting to resolve sound waves at high CFLs. Poorly resolved wavelengths are strongly damped and cannot be adequately represented. However, if only long wavelengths are of interest, BIC-FCT can provide a substantial gain over an explicit method.

A Two-Dimensional Problem

When BIC-FCT is applied in two dimensions, the same basic three-step procedure is used. In addition, we use time splitting in the two spatial dimensions to implement the explicit FCT predictor and energy corrector step. However, for the method to work, the elliptic pressure change equation must be solved in two dimensions.

The solution of the elliptic pressure change equation is a substantial part of the computional effort at each timestep. In one dimension, the finite-difference form of the pressure difference equation can be solved efficiently in $O(N)$ operations, where N is the number of grid points, using standard tridiagonal methods (for example, see Roache [19]). In two dimensions, it is important to have an efficient elliptic solver, and preferably one that is not limited to specific types

of problems with specific boundary conditions. In the calculation presented below we use a multigrid method, MGRID [18], which is very fast and requires $O(NlogN)$ operations. This method is suitable for the parallel processing in pipelined, parallel, and vector computers. It is straightforward to use any other suitable elliptic solver.

The two-dimensional Cartesian test problem was selected to demonstrate the ability of BIC-FCT to treat nearly incompressible swirling flows. A potential vortex with a central core was used as an initial condition in a square 10 m $\times$ 10 m region. The initial conditions correspond to the analytic solution of a line vortex with diffusion which is of the form [20]

$$V_{tangential} = \frac{c}{r}\left[1 - e^{-r^2/4\nu t}\right] ,$$

where c and ν are constants. The flow very rapidly adjusts to the presence of the walls, but this does not affect the flow close to the vortex center. In this test, a stretched 40 $\times$ 40 grid was used with the smallest cells 10 cm in size placed at the center of the vortex. The maximum velocity, at the start of the calculation, was 30 m/s. A conservative timestep of 1 ms was used. This should be contrasted to the 60 to 120 μs timesteps required for stability in a fully explicit method. In this nearly steady-state problem, the effects of pressure fluctuations are expected to be negligible. Therfore, we could use $\omega = 1$, the fully implicit method.

For flow visualization purposes, the lower half of the fluid has been marked and appears as the dark area in Fig. 6. In the absence of diffusion processes, either physical or numerical, this interface remains sharp as the fluid rotates at a constant velocity. Figures 7 and 8 show the position of the interface after 50 and 200 timesteps respectively. The interface between the marked and unmarked fluid is no longer sharp, due to numerical diffusion. The interface remains fairly sharp outside the core region.

The velocity decay is given in a more quantitative manner by the scatter plots shown in the next set of figures. Tangential and radial components of velocity are plotted as a function of distance from the vortex center. Crosses denote the velocity actually obtained from the program and the solid line provides a least squares fit of the data to the analytic solution of the vortex with

diffusion [20]. The initial condition is shown in Figs. 9a and b. Figures 10a, 10b, and 11a, 11b show the velocity after 50 and 200 timesteps, respectively. The peak tangential velocity decreases due to numerical diffusion. However, the effective diffusion coefficient is not a constant either in space or time which leads to an imperfect fit of the data to the analytic solution. Scatter in the tangential velocity at the same location is due to the nonuniform retardation caused by varying amounts of numerical diffusion. Since the flow is essentially incompressible, nonzero radial velocities are generated.

We now examine the time it takes to do one computational timestep. Table 1 shows a timing comparison between BIC-FCT and the standard module, JPBFCT, very similar to that described by Boris [4]. In fact, the explicit FCT predictor in BIC-FCT is similar to the corrector step of JPBFCT. The table shows that the computational time required per timestep compares extremely favorably to that for the explicit method, especially at the larger grid sizes.

IV. SUMMARY AND DISCUSSION

In this paper we have described the Barely Implicit Correction method, BIC, for calculating subsonic flows. As pointed out by Casulli and Greenspan, only the pressure and velocity terms in the momentum and energy equations respectively have to be treated implicitly. This is sufficient to remove the sound-speed limit on the timestep. We then manipulated the equations to yield a single implicit equation, which is solved for a correction to an explicit predictor step. BIC can be used with any spatial differencing scheme. BIC-FCT provides the accuracy of the high-order monotone flux-corrected transport method but allows the large timesteps possible with an implicit method.

A number of test problems showed that BIC-FCT maintains the desirable high-order monotone characteristics of the explicit FCT algorithm. First, we showed that it could propagate a contact discontinuity as well as the two-step JPBFCT. We also presented a two-dimensional example of a swirling flow.

The implicitness parameter, ω, plays an important role in BIC-FCT whenever sound waves and pressure oscillations are important in the solution. Damp-

ing is negligble for long wavelenths and timesteps when $\omega = 0.5$. When sound waves are not important, ω can be set to unity.

The major gain is that the timestep is no longer restricted by the sound speed. This improvement is achieved at little or no additional cost per timestep. The cost of solving the elliptic equation is recovered by the elimination of the half-step calculations in explicit FCT.

In two-dimensional problems, an efficient method of solution of the elliptic pressure equation is essential. The multigrid technique MGRID used here is among the fastest. However, the application of this technique to even modestly complicated geometries is not straightforward. Unstructured multigrid methods [21] should provide the necessary flexibility.

Equations (9), (10), and (16) are in conservative form. Since the pressure correction only appears as a gradient in the velocity correction, vorticity generation and transport are unchanged by BIC. Thus vorticity stays a local, convected quantity.

In summary, BIC-FCT has opened up the possibility of doing very accurate, very slow flow calculations in which compression is important. Future computational directions include extensions to finite elements [22] and to addition of other physical processes such as gravity, viscosity, and chemical reactions to simulate premixed flames, diffusion flames, and turbulent jets.

ACKNOWLEDGEMENTS

This work was sponsored by NASA in the Microgravity Science Program and by the Naval Research Laboratory through the Office of Naval Research. The authors would like to thank Rainald Löhner, Rick DeVore and Paul Woodward for their helpful suggestions.

REFERENCES

1. S. K. Godunov, *Mat. Sb.* **47** (1959), 271–306.
2. J. P. Boris, *in* "Computing as a Language of Physics", pp. 171–189, International Atomic Energy Agency, Vienna, 1971.
3. J. P. Boris and D. L. Book, *Meth. Comp. Phys.* **16** (1976), 85–129.
4. J. P. Boris, "Flux-Corrected Transport Modules for Generalized Continuity Equations," NRL Memorandum Report 3237, Naval Research Laboratory, Washington, D.C., 1976. (AD-A023 891)
5. P. Woodward and P. Colella, *J. Comp. Phys.* **54** (1984), 115–173.
6. M. R. Baer and R. J. Gross, "A Two-dimensional Flux-Corrected Transport Solver for Convectively Dominated Flows," SAND85-0613, Sandia National Laboratories, Albuquerque, New Mexico, 1986.
7. F. F. Grinstein, E. S. Oran and J. P. Boris, *J. Fluid Mech.* **165** (1986), 201-220.
8. K. Kailasanath, J. H. Gardner, J. P. Boris and E. S. Oran, *in* "Proceedings of the 22nd JANNAF Combustion Meeting," pp. 341–350, Pasadena, California, 1985, Vol. I, CPIA-PUB-432. (AD-A165 503)
9. R. W. MacCormack, *in* "Proceedings of the Second International Conference on Numerical Methods in Fluid Dynamics," (M. Holt, Ed.), pp. 151–163, Springer-Verlag, New York, 1971.
10. R. M. Beam and R. F. Warming, *AIAA J.* **16** (1978), 393–402.
11. C. W. Hirt, A. A. Amsden and J. I. Cook, *J. Comp. Phys.* **14** (1974), 227–254.
12. B. A. Fryxell, P. R. Woodward, P. Colella and K-H. Winkler, "An Implicit-Explicit Hybrid Method for Lagrangian Hydrodynamics," to appear in *J. Comp. Phys.* **63** (1986), 283-310.
13. H. C. Yee and A. Harten, *in* "AIAA 7th Computational Fluid Dynamics Conference," pp. 228–241, Cincinnati, Ohio, 1985.
14. W. W. Jones and J. P. Boris, *J. Phys. Chem.* **81** (1978), 2532–2534.

15. R. G. Rehm and H. R. Baum, *J. Research* (National Bureau of Standards) **83** (1978), 297–308.

16. S. Paolucci, "On the Filtering of Sound from the Navier - Stokes Equations," SAND82-8257, Sandia National Laboratories, Albuquerque, New Mexico, 1982.

17. V. Casulli and D. Greenspan, *Int. J. Num. Methods Fluids* **4** (1984), 1001-1012.

18. C. R. DeVore, "Vectorization and Implementation of an Efficient Multigrid Algorithm for the Solution of Elliptic Partial Differential equations," NRL Memorandum Report 5504, 1984. (AD-A149 049)

19. P. J. Roache, "Computational Fluid Mechanics," Hermosa, Albuquerque, New Mexico, 1972.

20. G. K. Batchelor, "An Introduction to Fluid Dynamics," Cambridge University Press, Cambridge, 1967.

21. R. Löhner and K. Morgan, "Unstructured Multigrid Methods: First Experiences," *in* "Proceedings of the Third International Conference on Numerical Methods in Thermal Problems," (R.W. Lewis et. al. Eds.), Pineridge Press, Swansea, 1985.

22. R. Löhner, K. Morgan, M. Vahdati, J. P. Boris and D. L. Book, "FEM-FCT: Combining Unstructured Grids with High Resolution," submitted to *J. Comp. Phys.*, 1986.

Table 1.

Timings* per Step of BIC-FCT and JPBFCT

	20 × 20	40 × 40	80 × 80
BIC-FCT			
explicit	6.8 ms	17.0 ms	54.1 ms
elliptic	3.8	8.4	22.5
other	2.7	5.9	17.1
total	13.3	31.3	93.7
per point	33.3 μs	19.6 μs	14.6 μs
JPBFCT	13.6 ms	33.9 ms	108.1 ms
per point	34.0 μs	21.2 μs	16.9 μs

* on CRAY XMP-12

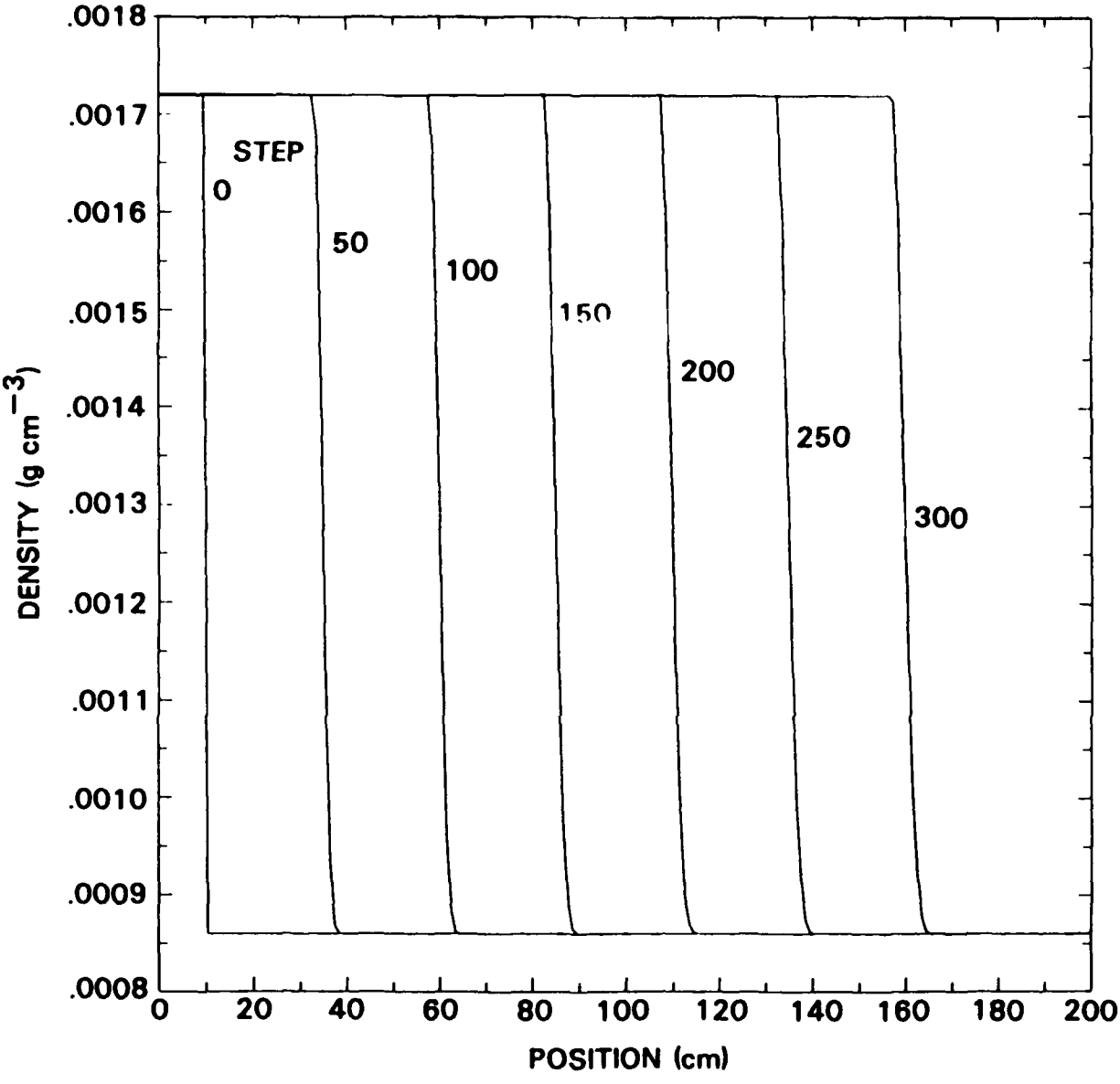

Figure 1 — Density profiles of a propagating contact discontinuity at 50 step intervals.

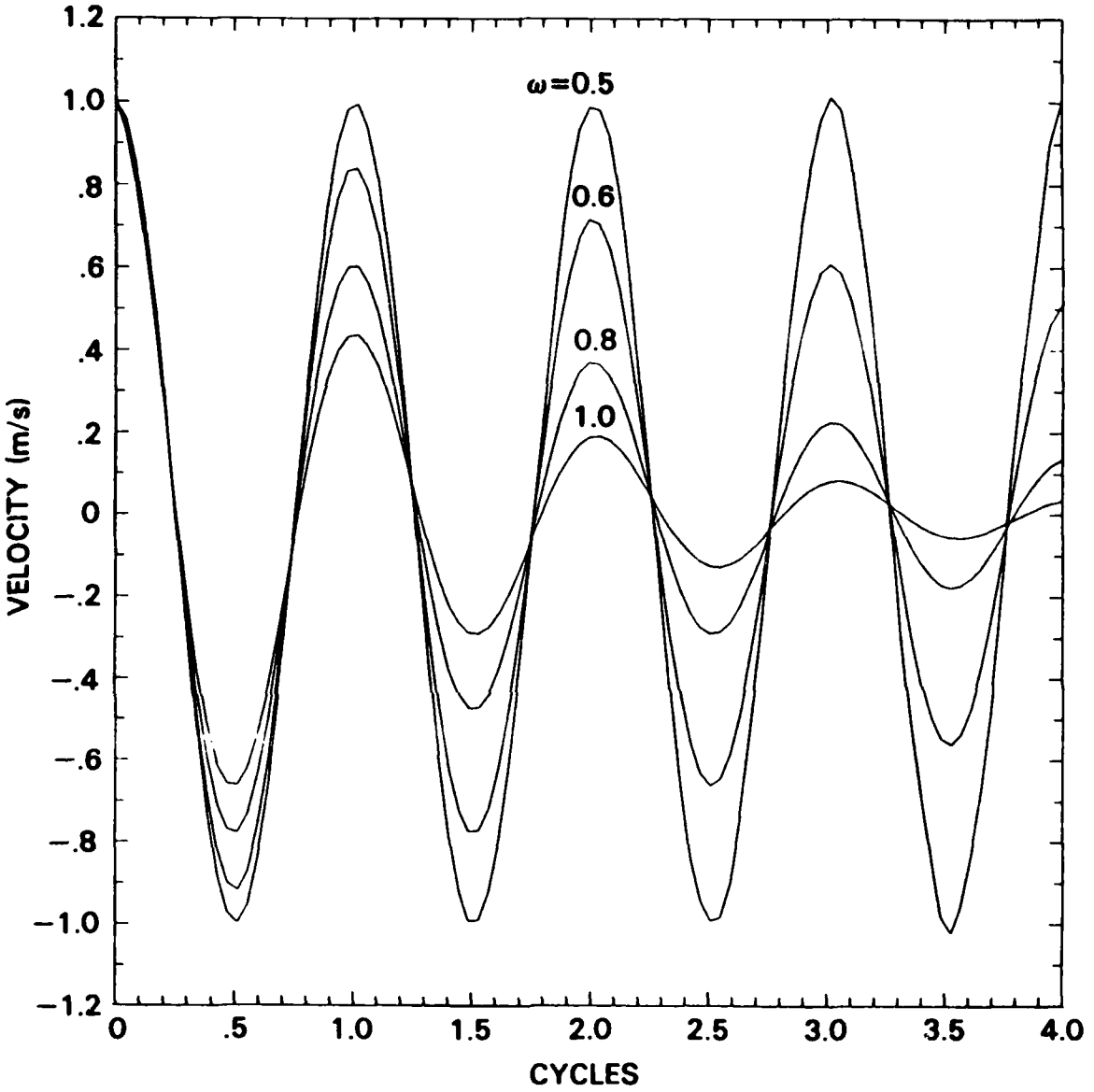

Figure 2 — Effect of ω on the damping of a sound wave.

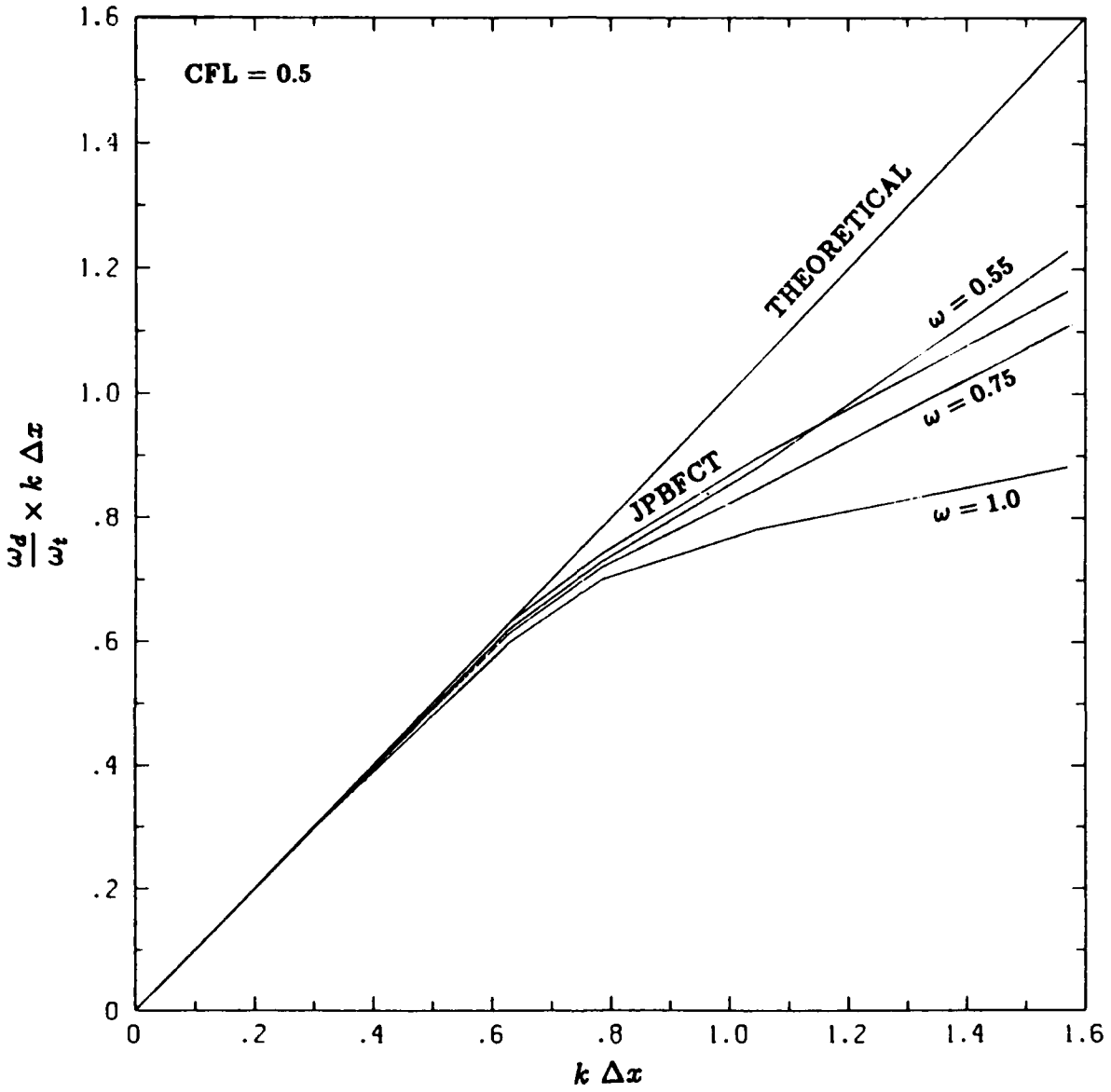

(a) dispersion relation

Figure 3 — Dispersion and damping of sound waves by BIC, *CFL* = 0.5.

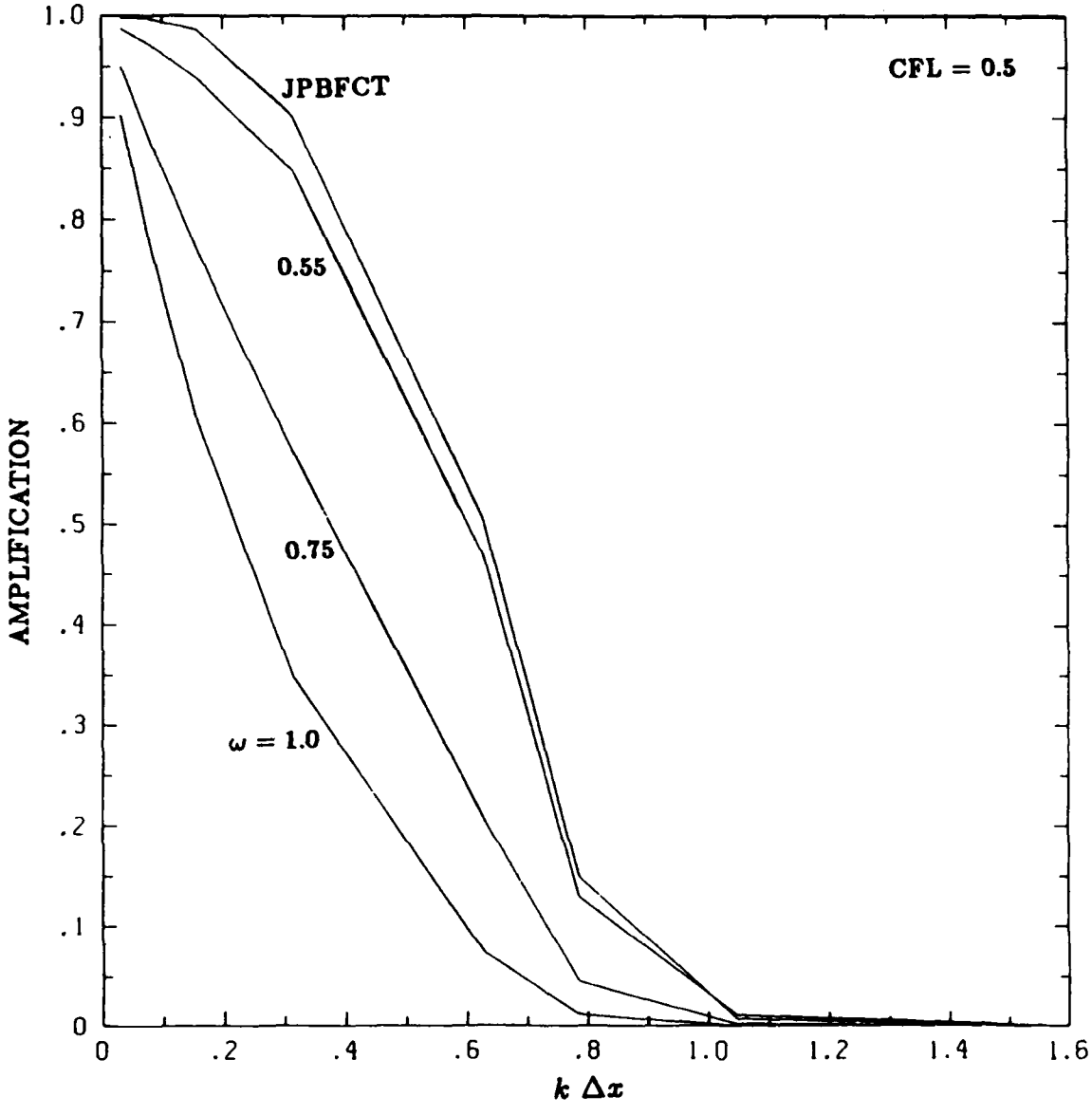

(b) damping rate

Figure 3 (Continued) — Dispersion and damping of sound waves by BIC, *CFL* = 0.5.

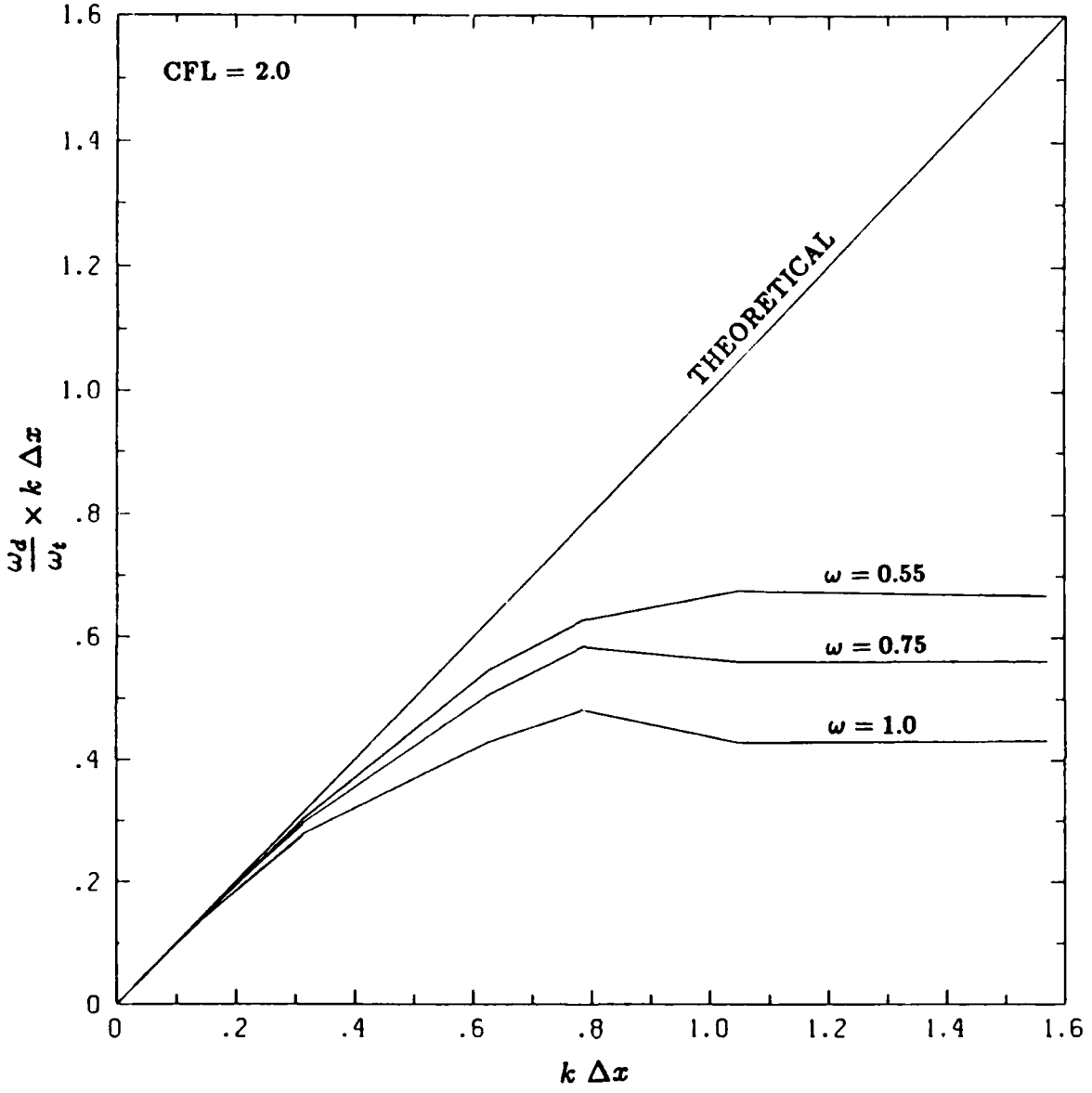

(a) dispersion relation

Figure 4 — Dispersion and damping of sound waves by BIC, *CFL* = 2.0.

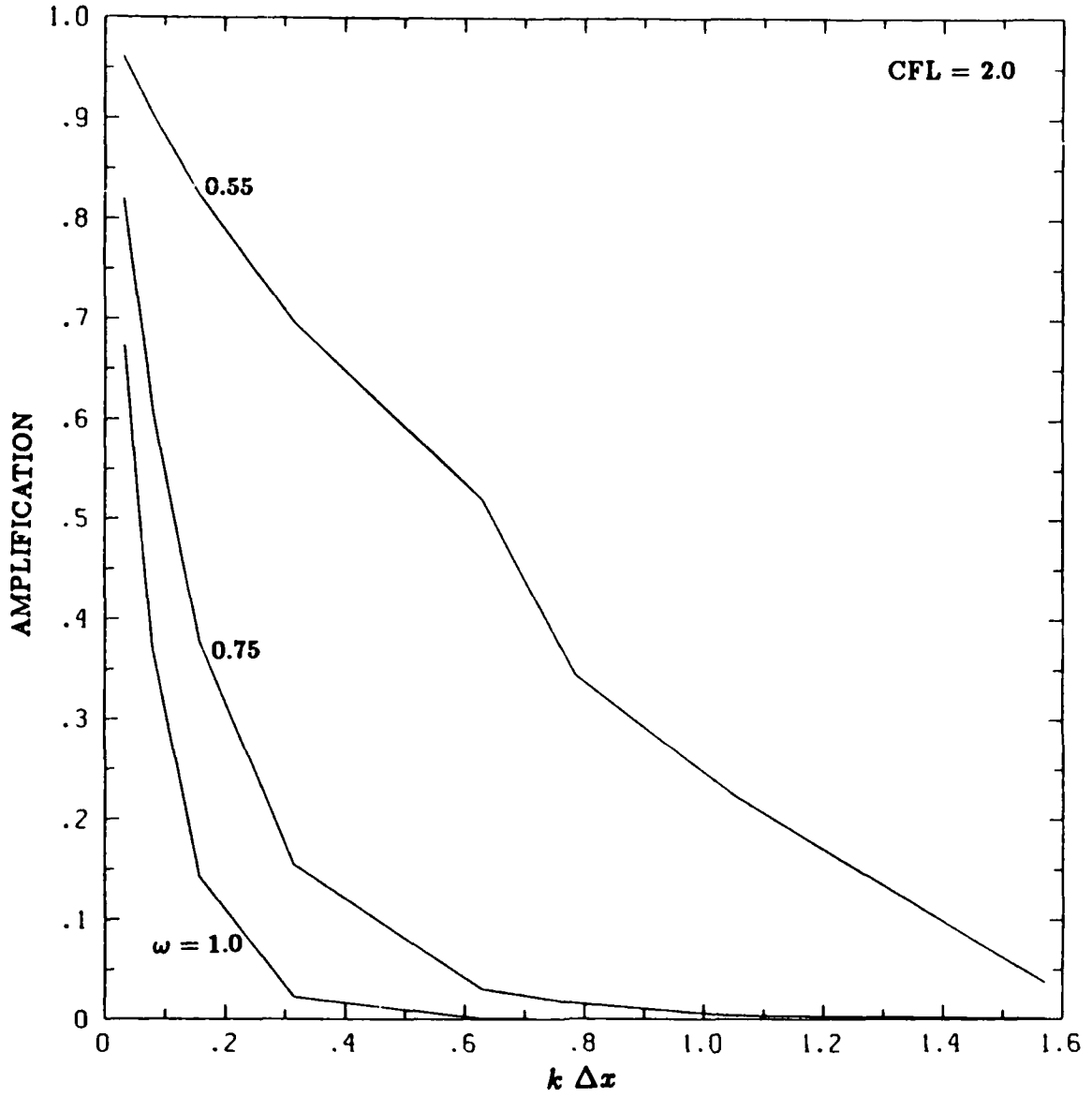

(b) damping rate

Figure 4 (Continued) — Dispersion and damping of sound waves by BIC *CFL* = 2.0.

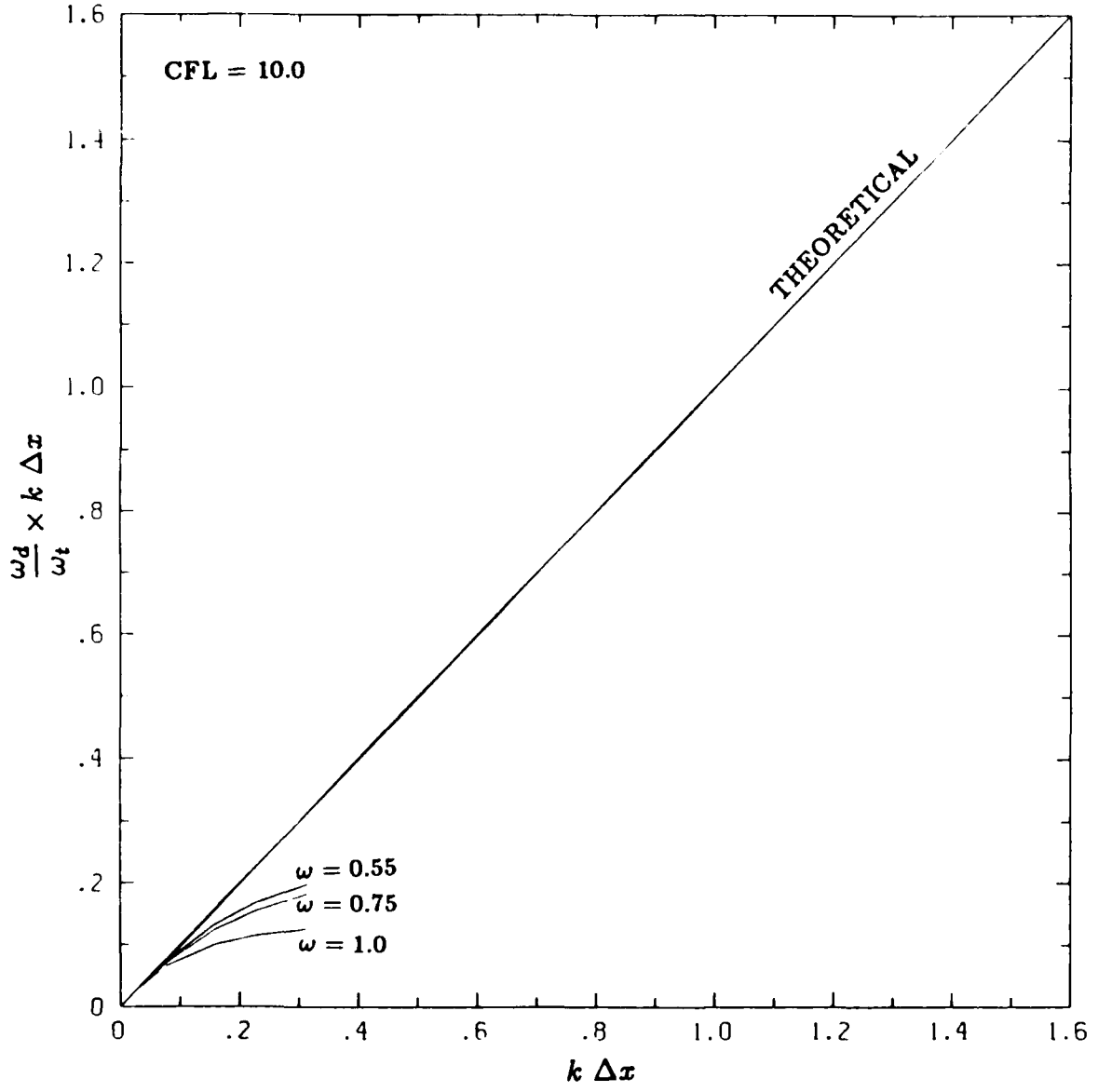

(a) dispersion relation

Figure 5 — Dispersion and damping of sound waves by BIC, *CFL* = 10.0.

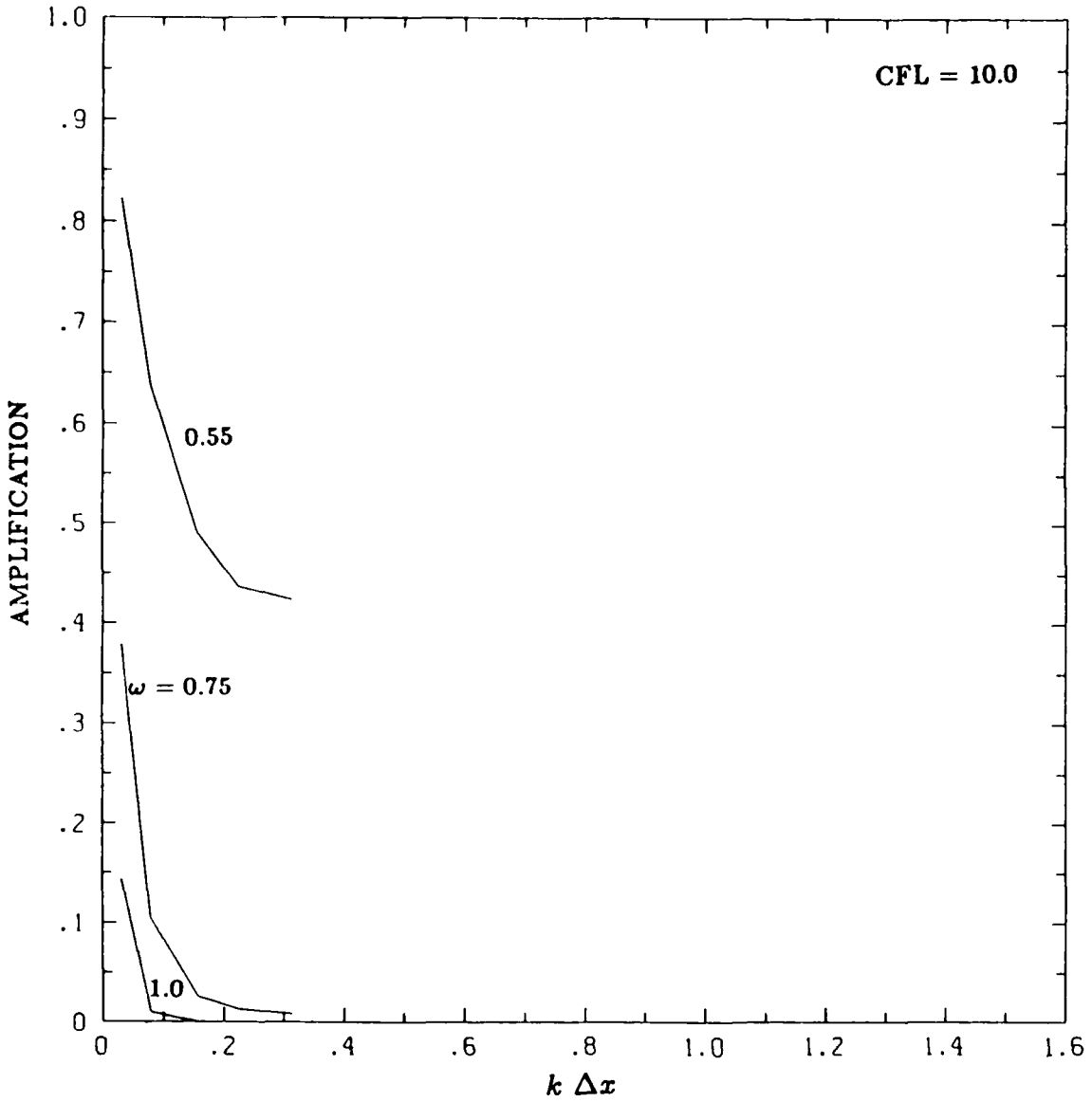

(b) damping rate

Figure 5 (Continued) — Dispersion and damping of sound waves by BIC, *CFL* = 10.0.

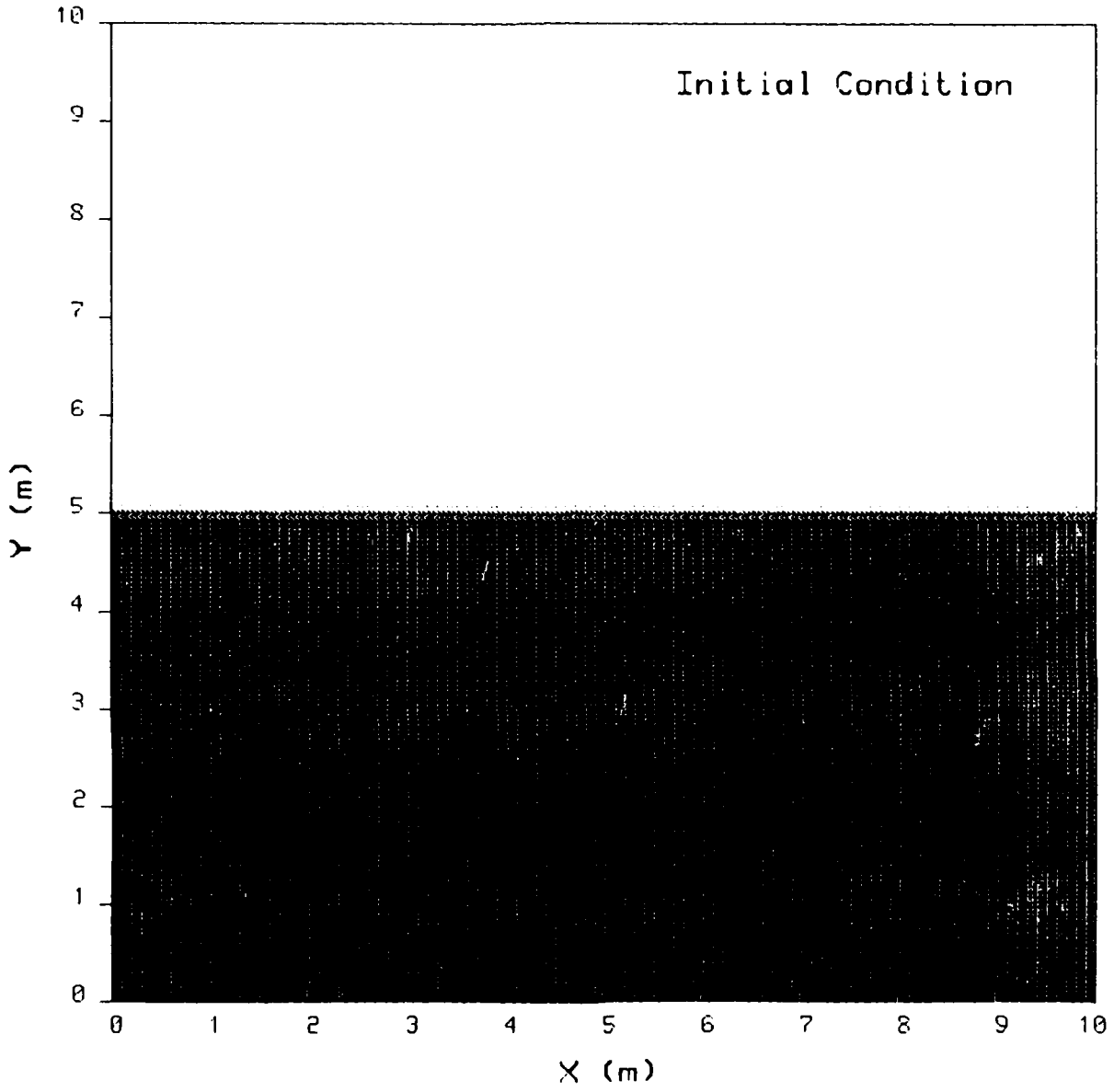

Figure 6 — Flow visualization of two-dimensional vortex flow, initial condition.

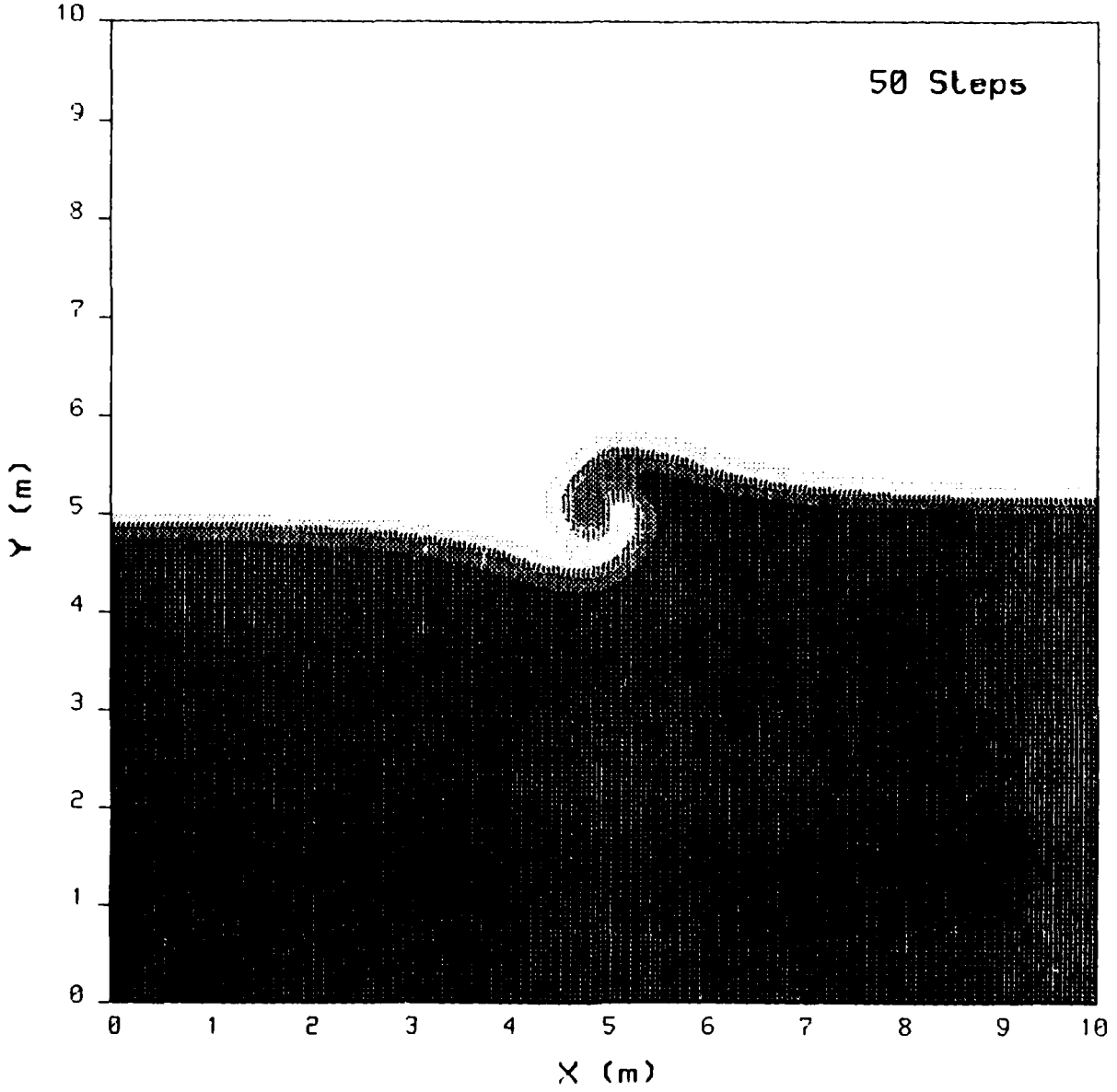

Figure 7 — Flow visualization of two-dimensional vortex flow, 50th step.

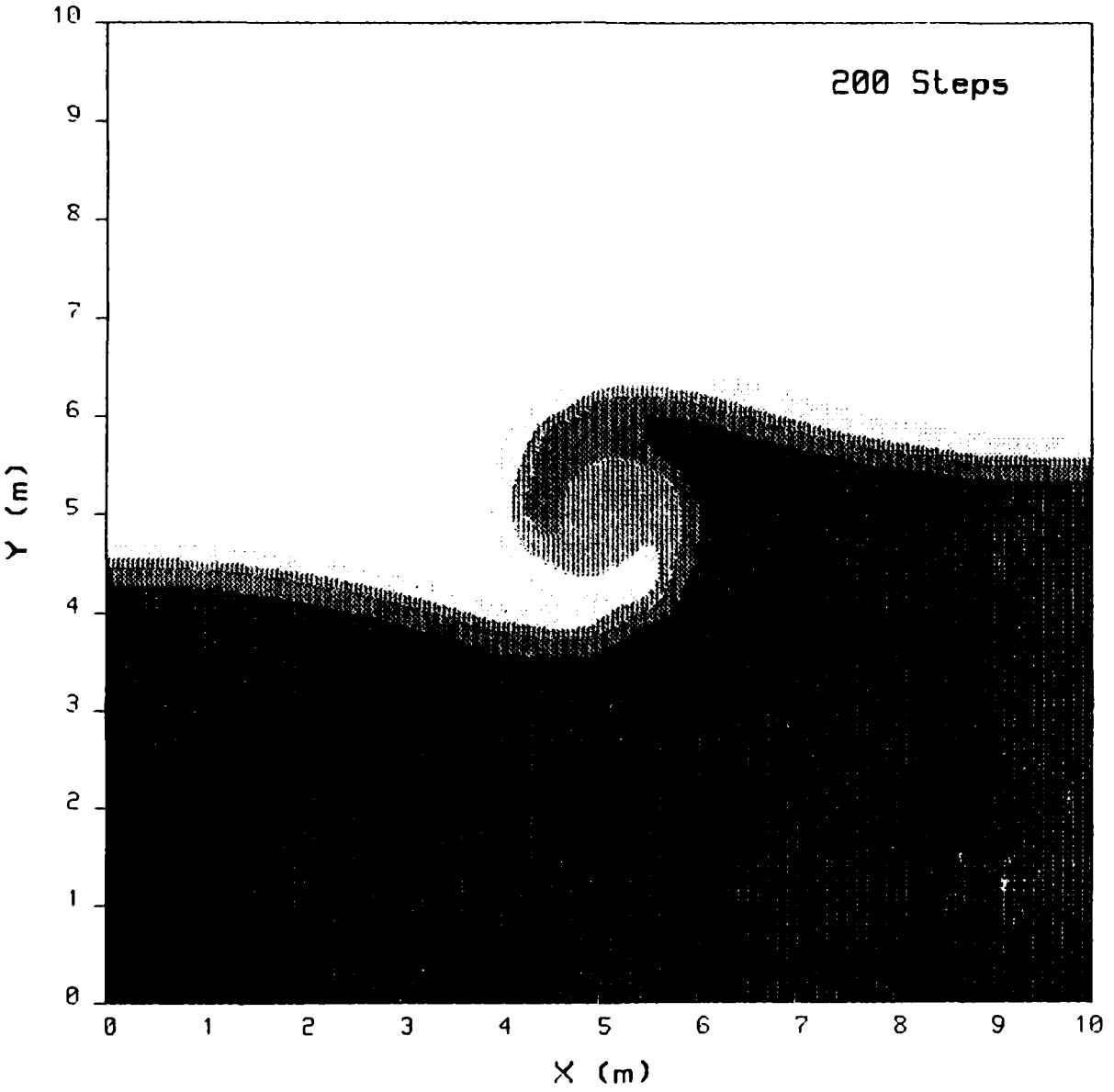

Figure 8 — Flow visualization of two-dimensional vortex flow, 200th step.

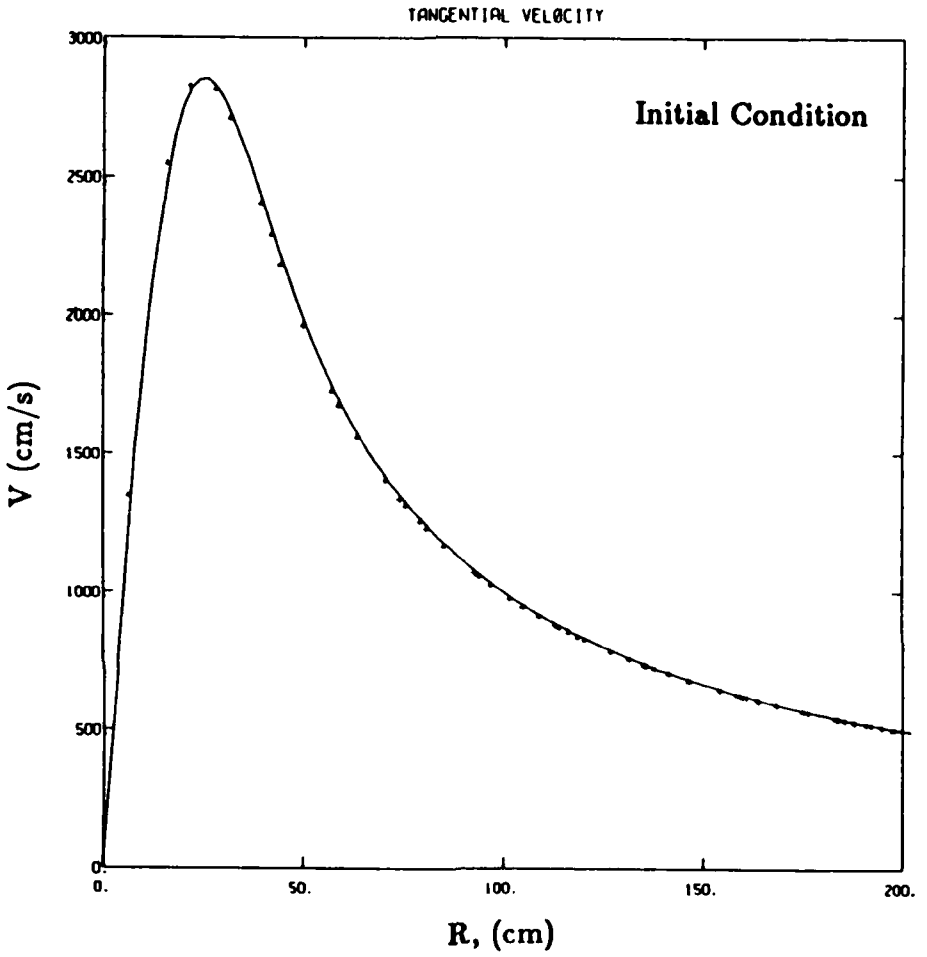

(a) radial component of velocity

Figure 9 — Scatter plot of velocity in vortex flow, initial condition.

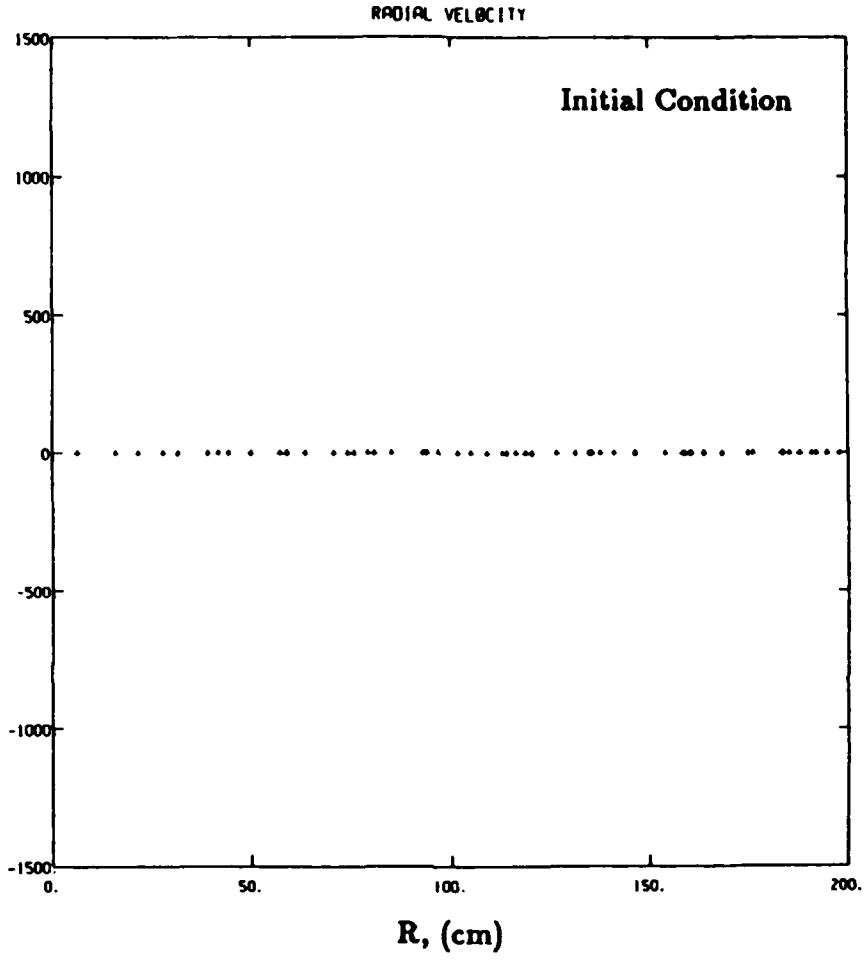

(b) tangential component of velocity

Figure 9 (Continued) — Scatter plot of velocity in vortex flow, initial condition.

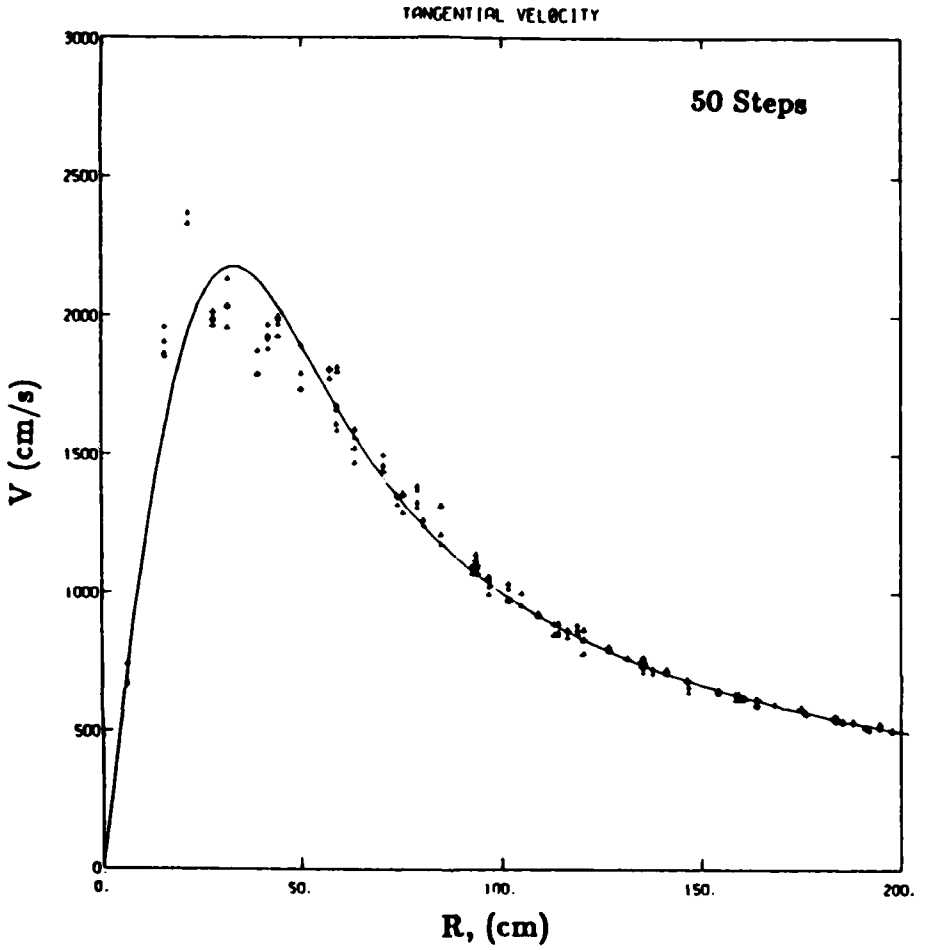

(a) radial component of velocity

Figure 10 — Scatter plot of velocity in vortex flow, 50th step.

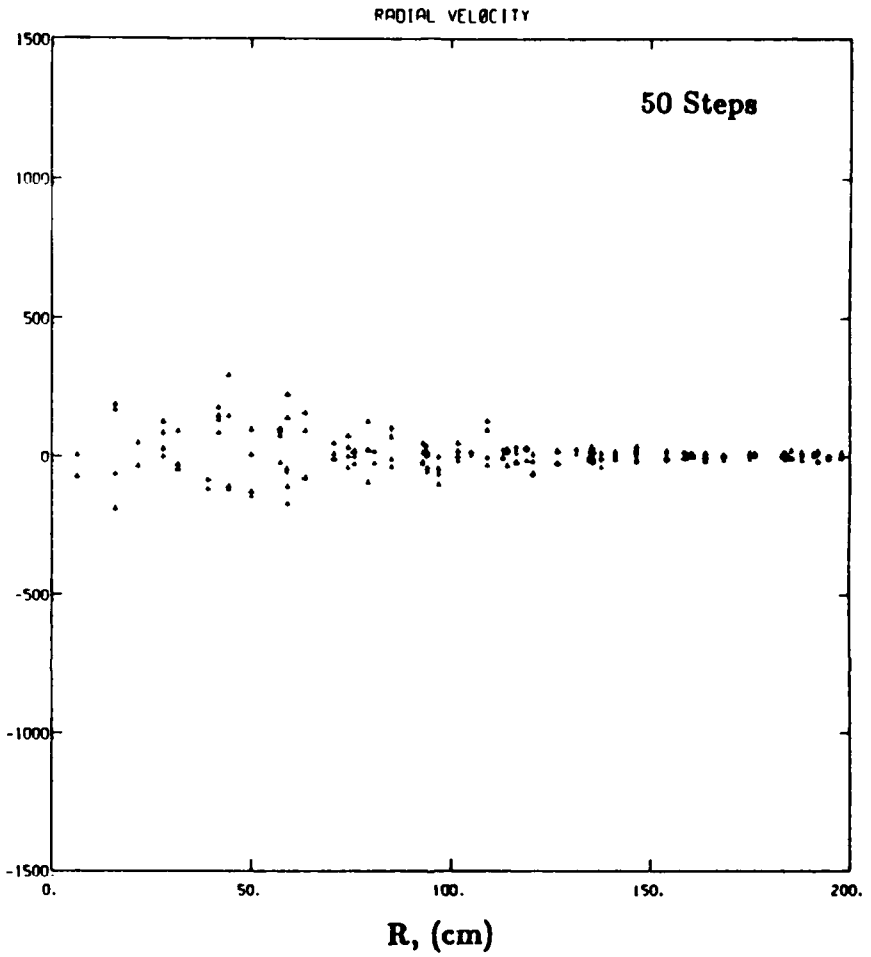

(b) tangential component of velocity

Figure 10 (Continued) — Scatter plot of velocity in vortex flow, 50th step.

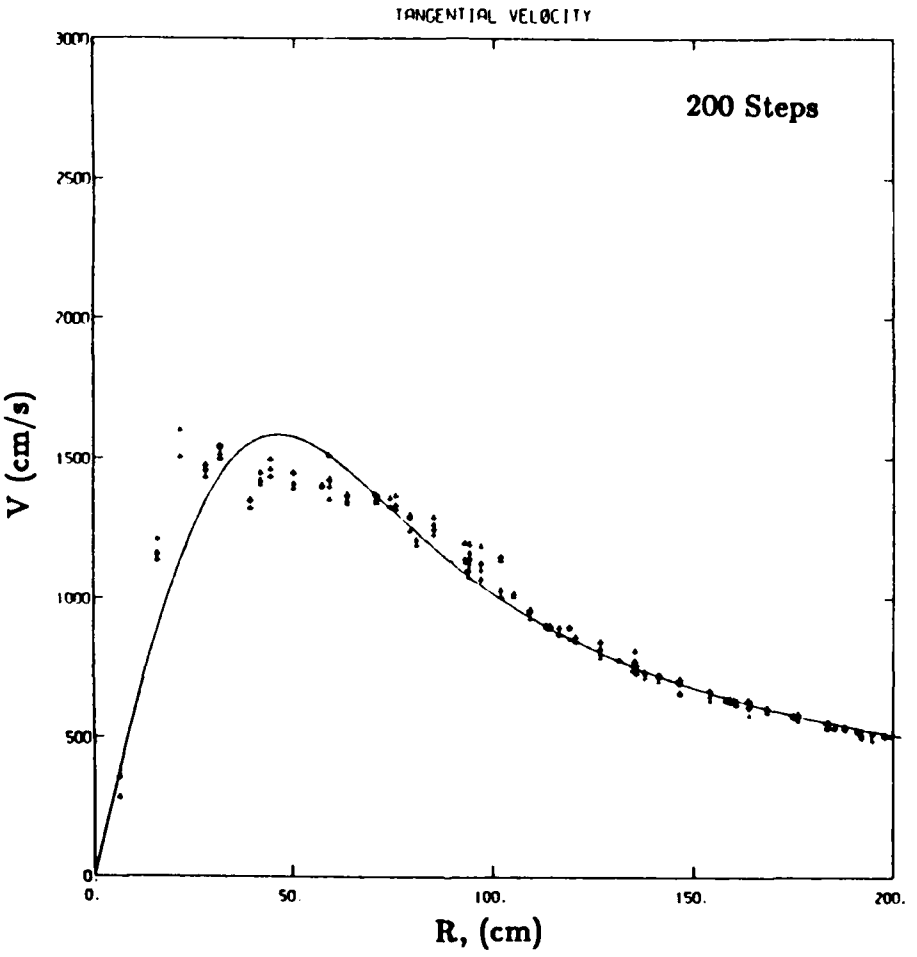

(a) radial component of velocity

Figure 11 — Scatter plot of velocity in vortex flow, 200th step.

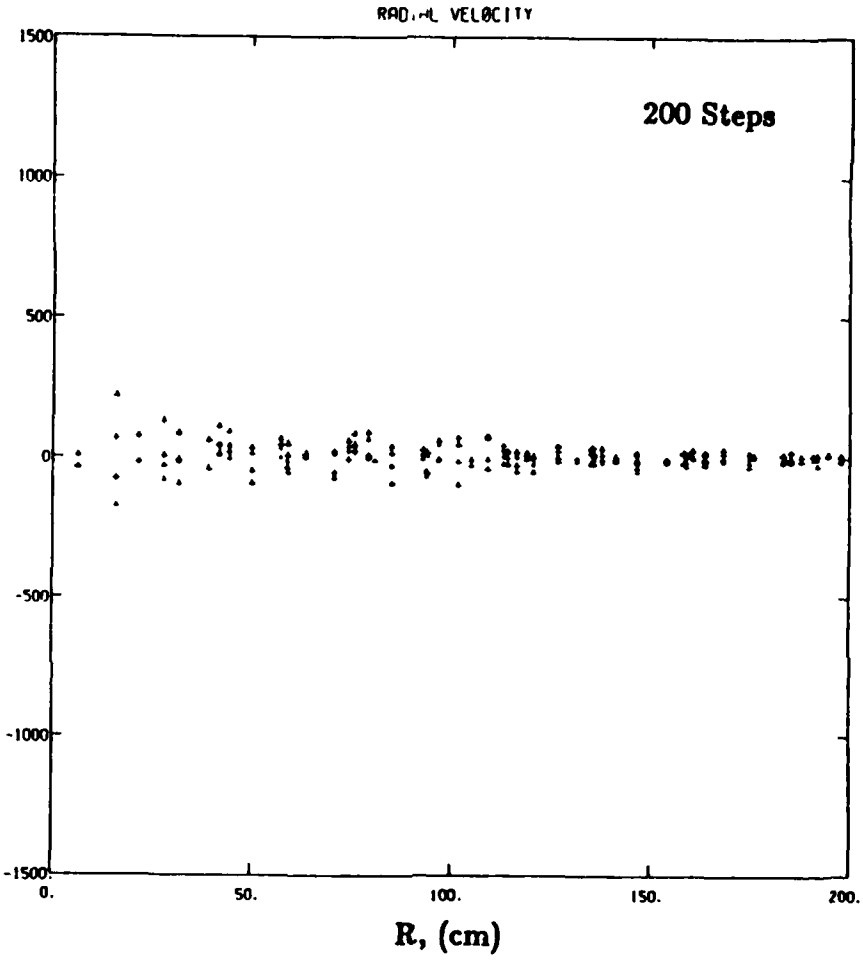

(b) tangential component of velocity

Figure 11 (Continued) — Scatter plot of velocity in vortex flow, 200th step.

END

12-86

DTIC